Proc Indian Natn Sci Acad, **71, A,** Nos. 1 & 2, January & March 2005, pp. 47–57

SPATIOTEMPORAL CHAOS AND SPIRAL TURBULENCE IN MODELS OF CARDIAC ARRHYTHMIAS: AN OVERVIEW

T K SHAJAHAN[1], SITABHRA SINHA[2] AND RAHUL PANDIT[1*]

[1]*Centre for Condensed Matter Theory, Department of Physics, Indian Institute of Science, Bangalore-560 012 (India)*

[2]*Institute of Mathematical Sciences, C I T Campus, Taramani, Chennai-600 113 (India)*

(Received 09 October 2003; Accepted 28 January 2005)

Ventricular fibrillation (VF), the major reason behind sudden cardiac death, is turbulent cardiac electrical activity in which rapid, irregular disturbances in the spatiotemporal electrical activation of the heart make it incapable of any concerted pumping action. Partial-differential-equation models of excitable media, based on reaction-diffusion equations, have proved to be very useful in the study of cardiac arrhythmias such as VF. We give an overview of such models, with special emphasis on the control and characterization of the spiral turbulence and spatiotemporal chaos that occur in them. Such spiral turbulence is associated with VF, so its control has implications for defibrillation schemes.

Key Words: Cardiac Arrhythmias; Spiral Turbulence; Spatiotemporal Chaos

1 Introduction

Ventricular fibrillation, the spontaneous, incoherent excitation of ventricular muscle fibres, is the most dangerous of all cardiac arrhythmias. It is the leading cause of death in many industrialized countries. It is estimated that, in the USA alone, more than 450,000 deaths occur because of cardiac arrhythmias, most often VF[1]. South Asians are more vulnerable to these arrhythmias, as suggested by recent clinical studies[2].

The mammalian heart is an electro-mechanical device which pumps blood via rhythmic contractions of the atria and ventricles. The walls of the atria and ventricles are excitable media that support the passage of regular contraction waves. The cardiac cells in these walls are threshold-activated devices which are excited when they receive a stimulus that exceeds a certain threshold value. In its quiescent state, a cardiac cell maintains a potential difference of $\cong -85$mV across the cell membrane. It becomes depolarized when stimulated electrically beyond a threshold potential: Ion channels on the membrane now allow the inward passage of Na^+ ions; this causes the cell to depolarize rapidly to voltages up to +40 mV. After this rapid-depolarization stage, as the sodium permeability of the membrane decreases, there is a very brief repolarization stage followed by a relatively longer steady state, called the *plateau region.* During this plateau phase, various other currents arising from Ca^{++} and K^+ ions are activated. Finally the cell returns to its resting-state value after a long repolarization phase. After excitation, the cell remains refractory to new stimuli for some time, i.e., it cannot be readily excited again. The rapid repolarization, the plateau region, and the repolarization phase is called the cardiac action potential, an illustrative example of which is shown in Fig. 1; this has been obtained from the Luo-Rudy model that we describe below.

Each cardiac cell is electrically coupled to its neighbours; hence the excitation of one region initiates a wave that propagates through the entire heart. Irregularities in the spatiotemporal behaviour of this system are manifested as cardiac arrhythmias. The visualization of cardiac arrhythmias by using voltage-sensitive dyes and CCD cameras has shed much light on this seemingly random fibrillation. Many groups have recorded the nature of wave propagation in cardiac tissue. Interesting observations include the presence of spiral waves or broken spiral waves during episodes of ventricular fibrillation[3]. Fig. 2 shows such a spiral wave induced artificially in a canine heart.

Spiral waves occur generically in excitable media. Such media are threshold-activated, spatially distributed systems which have the ability to propagate waves. They can be modelled by coupling a group of elements to each other, such that each element can pass information to its neighbours. Each element is characterized by a quiescent state that is stable with respect to small perturbations. A

*Also at Jawaharlal Nehru Centre for Advanced Scientific Research, Bangalore-560 064 (India)

[1]*E-mail:* shajahan@physics.iisc.ernet.in

[2]*E-mail:* rahul@physics.iisc.ernet.in

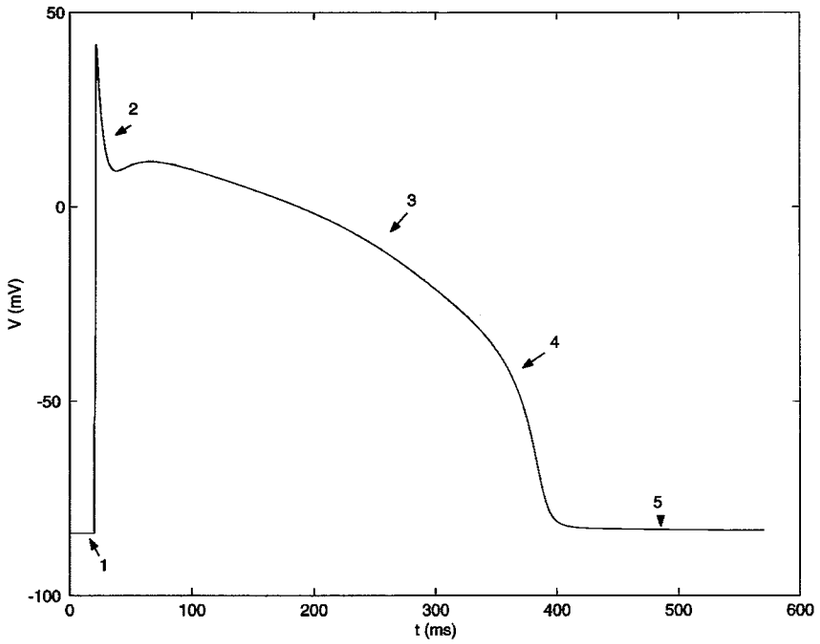

Fig. 1 An example of a cardiac action potential obtained from a single cell in the Luo-Rudy model (Appendix B) showing (1) the action potential upstroke or rapid depolarization, (2) the rapid repolarization, (3) the plateau stage, (4) the final stage of repolarization, and (5) the resting state, in a plot of transmembrane potential V versus time t.

Fig. 2 A spiral wave on a canine heart imaged using voltage-sensitive dyes and CCD cameras. (Image obtained from and reproduced with the permission of W. Ditto)

stimulus, with amplitude greater than a specific threshold, can cause the quiescent state of that element to undergo a large excursion from its resting value. It eventually returns to its rest state value. This sequence of events is known as excitation. The length of time required to return close to the resting state determines the refractory time of that point; a refractory element cannot undergo another excitation until it recovers. Excitation of one element will initiate excitation in its neighbouring elements because of the coupling between them. In homo-geneous excitable media, the wave of excitation moves out as an expanding circle. However, under certain conditions, these media can also sustain spiral waves.

Spiral waves form naturally when a wavefront travels around a pivot point and repeatedly excites itself; it is called a reentrant excitation since the wave reenters the region it has excited previously. Reentry can be of two types, anatomical and functional. In anatomical reentry, a cardiac impulse travels around a predetermined circuit (e.g., around an anatomical obstacle). Mines[4] was the first to study anatomical reentry in a ring of cardiac muscle which was obtained from a canine heart. Later studies[5,6] suggested that the presence of an anatomical obstacle is not essential for the initiation or maintenance of reentry. For instance, a wave break can occur because of a transient heterogeneity in the system and result in a spiral wave, even in an otherwise homogeneous medium. The resulting spiral wave may itself be unstable and it can break up further and create more spirals. This spiral break up provides a possible mechanism for the initiation of ventricular fibrillation. It involves the generation of complicated spatiotemporal patterns in an excitable medium arising from instabilities in wave propagation. The resulting spiral turbulent state, an instance of spatiotemporal chaos, is characterized by many positive Lyapunov exponents[7]. The number of positive Lyapunov exponents increases with the system size.

Apart from cardiac tissue, rotating spiral waves are frequently observed in homogeneously and heterogeneously catalyzed chemical reactions[8] and various biological systems, including, slime-mould aggregation[9], calcium waves in frog eggs[10], etc. All these systems exhibit spiral breakup and can be modelled by reaction-diffusion systems which are coupled, nonlinear, partial differential equations that describe the spatiotemporal evolution of concentration fields. This suggests that ventricular fibrillation can also be studied in the context of spatiotemporal chaos in reaction-diffusion systems[11,12]. Reaction-diffusion models of the cardiac action potential are of the form

$$\frac{\partial V}{\partial t} = D\nabla^2 V - \frac{I_{ion}}{C}. \qquad ...(1)$$

Here V is the transmembrane potential, C is the membrane capacitance, D, the diffusion coefficient, is related to the conductivity of the cardiac tissue, and I_{ion} is the total ionic current passing across the membrane. Different models of the cardiac action potential differ in the details of the ionic current. Two important models of this type, namely, the Beeler-Reuter (BR) and Luo-Rudy (LR) models are defined in details in Appendices A and B, respectively.

In the next Section we give some details about the models used to study the dynamics of cardiac arrhythmias. We also describe the spiral turbulence and spatiotemporal chaos observed in such models. In Section 3 we look at some of the methods proposed for controlling spiral turbulence in these models. Section 4 contains concluding remarks about the implications of these studies for developing more effective methods for treating cardiac arrhythmias.

2 Models

Early mathematical work by Rushton[13] and Kolmogorov *et al.*[14] addressed the question of wave motion in an excitable medium, long before there was a basic understanding of the nature of excitability in cardiac and nerve cells. The development of voltage-clamp techniques by Cole[15] allowed the detailed mechanism of cardiac functioning to be traced at the cellular level. In 1952 Hodgkin and Huxley[16] proposed the first quantitative model of wave propagation in a squid giant axon. On the basis of this, Noble[17] developed in 1962 the first physiological model of Purkinje fibres. Further studies in this field resulted in the development of several realistic ionic models of cardiac tissue derived from voltage-clamp and patch-clamp experiments[18]. Such ionic models accurately reproduce most of the basic properties of cardiac tissue, like depolarization and repolarization phases of the action potential, restitution properties, dynamical changes in the ionic concentration, etc. However, these ionic models are computationally expensive to simulate, when we take into account spatial coupling over large simulation domains, necessary, e.g., in studies of cardiac arrhythmias. Hence some groups have introduced simplified models with just two or three variables. These are the FitzHugh-Nagumo[19] (FHN) and related models, which permit us to develop some amount of

analytical understanding of cardiac arrhythmias; and they are also numerically effective for studying the propagation of spiral waves in two- and three-dimensional simulation domains, even with anatomically correct geometries. Both types of models, i.e., the detailed physiological models and the simplified FHN-based models, exhibit spiral turbulence in certain parameter regimes and for certain classes of initial conditions.

Apart from models of the reaction-diffusion type [eq. (1)] there are also cellular-automata models of the cardiac action potential[20]: cardiac tissue is modelled as a cellular automaton in which "cells", arranged in a grid, can exist in a number of discrete states, and the state of a particular cell is determined by a set of rules. This approach was used in earlier models of action-potential propagation in cardiac tissue[21], and in studies of fibrillation and other arrhythmias[22,23], since cellular-automation models are computationally more attractive than biophysically accurate models. However, this advantage is being lost because of the rapid increase in computer power over the last decade[24].

(A) Spiral Turbulence in Physiological Models

Electrical-wave propagation in cardiac tissue is usually modelled by cable equations. Such equations ignore discontinuities in the tissue because of the microscopic cell structure. If the tissue is treated as a continuous system, the transmembrane potential V follows the reaction-diffusion equation (1). Beeler and Reuter proposed a detailed ionic model, based on Noble's model for Purkinje fibres, for the action potential in the ventricular myocardium[18]. The model incorporates two voltage- and time-dependent inward currents which move into the cell, the excitatory sodium current, and a slow inward current primarily carried by calcium ions. The outward currents include a time-independent potassium current and a voltage- and time-dependent current primarily carried by potassium ions. With the development of single-channel measurement techniques, the BR model was improved by Luo and Rudy (LR)[25]. This model takes into account details of the outward, time-independent, potassium current and thus is able to explain properties like supernormal excitability, Wenckebach periodicity[26], etc. Even more realistic and more complicated models have been developed with the improvement of experimental techniques[27]. Here we restrict ourselves to the BR and LR models since they exhibit most of the properties of the cardiac action potential in which we are interested.

All these models are based on the Hodgkin-Huxley formalism in which the ion channels can be either open or closed. The total current I_{ion} is a sum of currents through various ion channels. And the current through a specific ion channel x can be described as $I_x = f_x I_{x,max}$, where f_x is the fraction of the total population of channels of type x in the open state, and $I_{x,max}$ is the maximum possible current through the channel. The state of a single channel i is controlled by a number of gates which we will denote by n_i. A channel is in the open state if all the gates of the channel are open. Each gate behaves independently of the other gates. The gates open or close at a rate determined by the first-order differential equation

$$\frac{dn_i}{dt} = (1 - \alpha_{ni})\, \mathrm{n}_1 - \beta_{n_i} n_i \qquad ...(2)$$

where the rate constants α_{n_i} and β_{n_i} are functions of the transmembrane potential. Details of both BR and LR models are given in Appendices A and B, respectively. In the BR model the rate constants for two of the gating variables depend on a parameter σ. It has been shown that[28], if σ is varied from 0.5 to 1, there is an onset of spiral break up in the BR model.

Spiral turbulence has also been observed in the LR model[7] (see Fig. 3). The spatial derivative in the Luo-Rudy equations is evaluated by a using a finite-difference scheme with a five-point stencil for the Laplacian (space step of δx = 0.002 cm); for time marching we use the forward-Euler method with a time step of δt = 0.01 ms. No-flux (Neumann) boundary conditions are used on the edges of the simulation domain. The model is initialized by a constant voltage of –84 mV, in a 400 × 400 simulation domain. To stimulate the domain, a plane wave is initiated in the domain by applying a stimulation current of 150μA/cm^2 for 1 ms at the top boundary. As this plane wave moves in to the bottom boundary, 285 ms after the first stimulus, a second stimulation of 150μA/cm^2 is given on the left boundary for 0.45 ms. We give a final stimulus at 465 ms with the same amplitude and duration on the top boundary. This causes the formation of a spiral tip. The resulting spiral wave becomes prominent by 665 ms; at this time we change the conductivity D from 0.001 to 0.0005, and the spiral wave that is formed breaks up and a spatiotemporally chaotic state is obtained by 850 ms.

(B) Spiral Breakup in the Panfilov Model

The Panfilov model is based on the FHN equations. It consists of two coupled partial differential equations

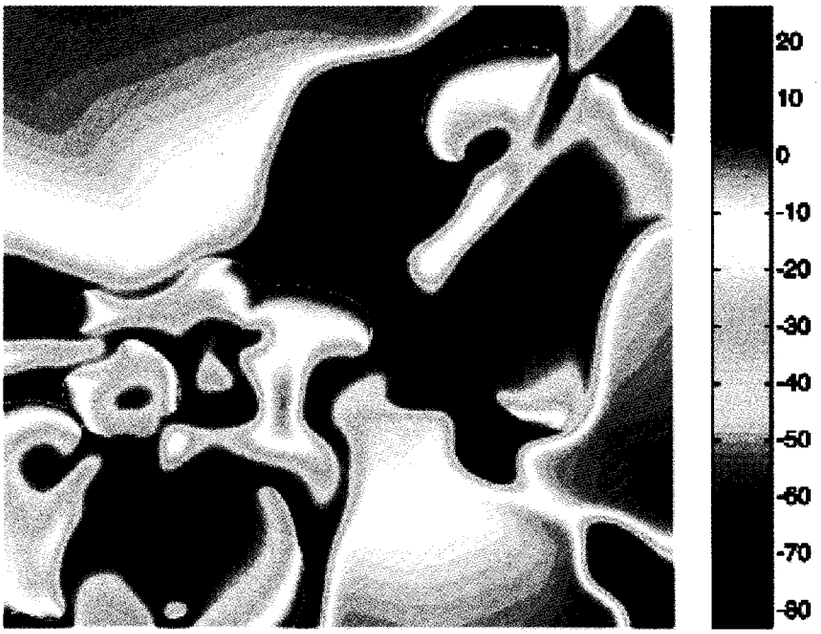

Fig. 3 Pseudocolour plot of the transmembrane potential V at points (x,y) in the 400 × 400 simulation domain illustrating spiral turbulence in the two-dimensional Luo-Rudy model.

(PDEs) for the fields $e(\mathbf{x},t)$ and $g(\mathbf{x},t)$. The e field, called the activation variable, represents the transmembrane potential of the ventricular cells at point $\mathbf{x}$ and time t. The g field, called the recovery variable, represents the membrane conductance at the same point; all information about the ion channels is contained in this field g. The model is

$$\partial e/\partial t = \nabla^2 V - f(e) - g, \qquad \partial g/\partial t = \in(e,g)\,(ke - g). \qquad ...(3)$$

Here $f(e)$ specifies fast processes (e.g., the initiation of the action potential) and is piecewise linear: $f(e) = C_1 e$, for $e < e_1$, $f(e) = -C_2 e + a$, for $e_1 \le e \le e_2$, and $f(e) = C_3 (e - 1)$, for $e > e_2$. The physically appropriate parameters given in Refs. [29,30] are $e_1 = 0.0026$, $e_2 = 0.837$, $C_1 = 20$, $C_2 = 3$, $C_3 = 15$, $a = 0.06$, and $k = 3$. The function $\in(e,g)$ determines the dynamics of the recovery variable: $\in(e,g) = \in_1$ for $e < e_2$, $\in(e, g) = \in_2$ for $e > e_2$, and $\in(e,g) = \in_3$ for $e < e_1$ and $g < g_1$, with $g_1 = 1.8$, $\in_1 = 1.75$, $\in_2 = 1.0$, and $\in_3 = 0.3$.

We integrate eq. (3) by using the forward-Euler method with a time step $\delta t = 0.022$ and a finite-difference method in space with a spatial step $\delta x = 0.5$ and a five-point stencil for the Laplacian. The dimensioned time T is defined to be 5 ms times the dimensionless time, and 1 spatial unit to be 1 mm, such that the period and wavelength of a spiral wave are approximately 120 ms and 32.5 mm, respectively. The dimensioned value of the conductivity constant is 2 cm^2/s. We use Neumann boundary conditions.

Let us now explore how spiral turbulence is obtained in the Panfilov model. The model is initialized with a broken wave front: For a system of linear size L at time $t = 0$ we set $g = 2$, for $0 \le x \le L$ and $0 \le y \le \frac{L}{2}$, and $g = 0$ elsewhere, and $e = 0$ everywhere except for $y = \frac{L}{2} + 1$ and $0 \le x \le \frac{L}{2}$, where $e = 0.9$. Spiral turbulence is observed when the linear system size L is greater than 128 mm and $\in_1 = 1/75$. The onset of spatiotemporal chaos and spiral turbulence in the Panfilov model is illustrated in Fig. 4. As $\in_1$ decreases, the pitch of the spirals decreases till states with broken spirals are obtained[31].

For example, if $\in_3 = 0.3$ and $\in_1 \ge 0.02$, eq. (3) displays rigidly rotating spirals; but if $\in_1 \cong 0.01$, a state containing broken spirals is obtained. This breaking of spirals is associated with the onset of spatiotemporal chaos as can be seen qualitatively from local phase portraits (plots in the $e - g$ plane of $(e(\mathbf{x},t_n), g(\mathbf{x},t_n))$ for fixed spatial coordinate $\mathbf{x}$ and regularly spaced times t_n). Rigidly rotating spirals lead to a periodic temporal evolution, so their phase portraits show all trajectories collapsing onto a single curve. As spiral break up occurs these points start to scatter (see Ref. [7]) indicating the onset of spatiotemporal chaos. Strictly speaking this chaotic behaviour is a transient of spatially and

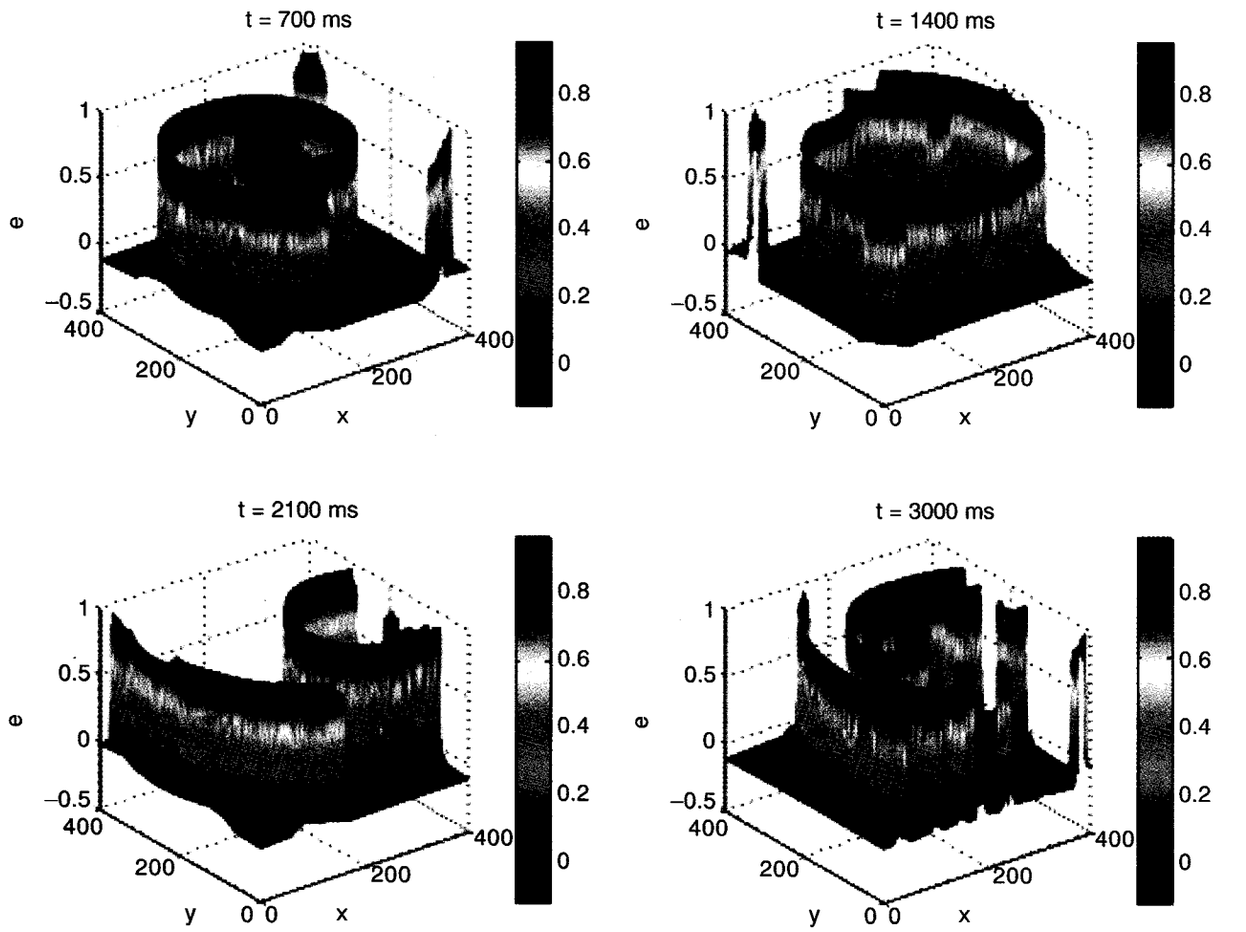

Fig. 4 Pseudocolour mesh plots for the field e as a function of the spatial coordinates x and y at different times t = 700 ms, t = 1400 ms, t = 2100 ms, and t = 3000 ms for $\in_1 = 0.01$ illustrating formation and break up of spiral waves in the Panfilov model [eq. (3)]. A broken-wave initial condition (see text) is used at $t = 0$. This leads to the creation of a spiral wave which breaks down as time increases leading to spiral turbulence with spatiotemporal chaos.

temporally irregular behaviour whose duration τ_L increases with the linear size L of the system. Fig. 5 shows the maximum Lyapunov exponent λ_m at time t versus t for $L = 128$ indicating that $\tau_{L=128} \cong 2200$. For time $t > \tau_L$, a quiescent state with $e = g = 0$ is obtained. In systems with $L > 128$, τ_L is sufficiently long that a nonequilibrium statistical steady state, displaying spatiotemporal chaos, is established. Several positive Lyapunov exponents have been reported in this state. The number of positive exponents increases with L as does Kaplan-Yorke dimension D_{KY}[12,32].

3 Controlling Cardiac Arrhythmias

The usual clinical method of controlling cardiac arrhythmias is the application of a massive electrical shock, of the order of ~ 100 – 1000 volts, across the heart. This is believed to reset the cardiac rhythm for all the cells at the same time. However, such defibrillation works only about two-thirds of the time and often damages the heart in the process of reviving it[33]. Recent theoretical studies of cardiac arrhythmias in model systems have viewed the spiral turbulence associated with these arrhythmias as a manifestation of spatiotemporal chaos. This has shed new light on the problem and led to the suggestion of some control algorithms which are potentially useful for low-amplitude defibrillation.

Low-dimensional chaos control makes use of the fact that, if a system's trajectory in state space comes very close to an unstable fixed point, it stays for a small duration of time in the neighbourhood of that point. Different methods have been proposed to drive chaotic trajectories towards an unstable fixed point, so that the system can stay in the neighbourhood of the fixed point

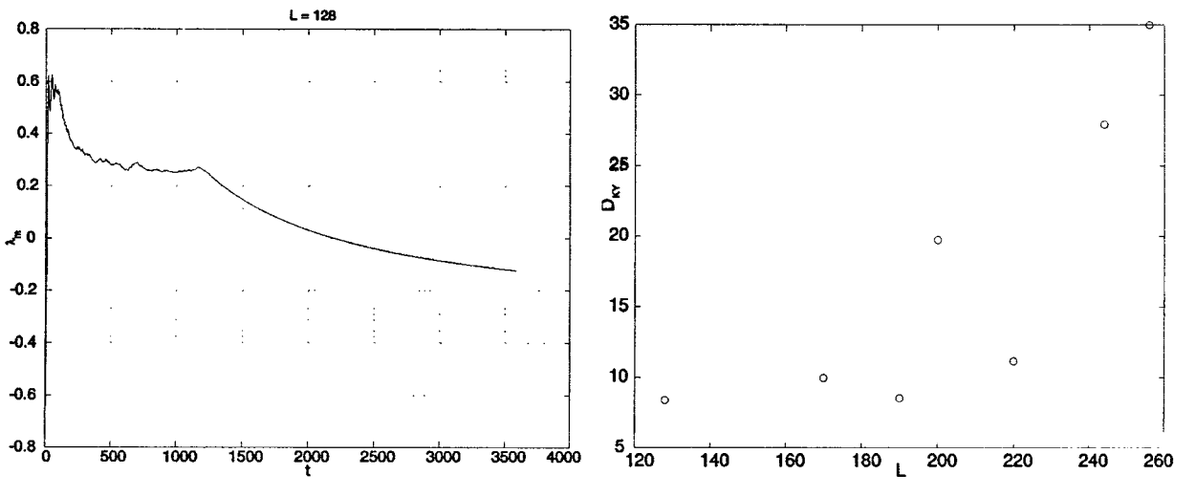

Fig. 5 The maximum Lyapunov exponent at time t versus t (left) for the Panfilov model. λ_m is positive in the beginning, and decays at large times to negative values indicating a long-lived chaotic transient which finally dies down to a quiescent state with $e(\vec{x},t) = 0$ and $g(\vec{x},t)$ everywhere. The Kaplan-Yorke dimension D_{KY} in the spatiotemporally chaotic transient versus the linear system size L is plotted on the right side.

for the duration of the control stimulus[34]. But ventricular fibrillation, which is a spatiotemporally chaotic state, and so intrinsically associated with a high-dimensional state space, cannot be controlled by low-dimensional control algorithms.

Biktashev and Holden[35] have proposed a method for controlling spiral turbulence by producing a directed movement of a rigidly rotating spiral wave from the medium by using resonant stimulation. They find that small-amplitude, spatially uniform, repetitive stimulations can be used to produce a directed movement of the spiral wave, if the period of stimulation is equal to the period of rotation of the spiral wave. This directed movement eventually pushes the spiral out of the simulation domain used in ref. [35]. However, this method can only be used before the onset of spiral turbulence.

Osipov and Collins[36] have suggested another scheme, based on the observation that the dynamics of excitable media can be separated into fast and slow variables, which can be considered separately. They control the slow variable by applying a weak impulse on the whole medium. This eventually changes the velocities of the wave front and the wave back. The propagation of the wave front and wave back with different velocities leads to a shrinkage or expansion of the pulse width. If the amplitude and time duration of the impulse is sufficiently large, then the propagating pulse collapses and disappears. Unfortunately such control of the slow variable over the whole medium can be achieved only by pharmaceutical means and not by the application of electrical pulses.

Rappel *et al.*[37] have proposed another method based on the application of a small control current at a finite number of equally spaced "controlled cells" in a tissue, by using a coarse lattice of electrodes with a lattice spacing of about 1 cm. This method has been demonstrated to prevent one spiral from breaking up. Unfortunately this method fails in the fully developed turbulent state with broken spirals.

To suppress a spatiotemporally chaotic state with broken spirals, Sinha *et al.*[7] have proposed a scheme based on the observation that spiral turbulence does not persist in the hearts of small mammals, if at all it can be initiated[38]. To construct an efficient defibrillation scheme for VF in the Panfilov model they noted the following points: (a) VF in such models of cardiac dynamics arises because the system evolves to a state in which large spirals break down[29]. (b) The VF state is a long-lived transient whose life time increases rapidly with the linear size of the system; e.g., in the two-dimensional Panfilov model for $L = 100$ mm, the lifetime of the spiral is $\cong 850$ ms, whereas for $L = 128$ mm, the lifetime increases to 3200 ms. (c) For large systems (system size $L > 128$ mm), the lifetime τ_L is sufficiently long so that a nonequilibrium statistical steady state is established. This state displays spatiotemporal chaos because the number of positive Lyapunov exponent increases with system size[7,12]. Since the long transient which leads to VF in the Panfilov model is spatiotemporally chaotic, we might guess that the fields e and g have to be controlled globally as in the method suggested by Osipov and Collins[36]. But in the control algorithm proposed in ref. [7], it is seen

that a judicious choice of control points on a mesh leads to an efficient defibrillation scheme. In this method, the simulation domain (of size $L \times L$) is divided into K^2 smaller blocks by a mesh of line electrodes, and the mesh size is chosen to be small enough that spirals cannot persist for long inside the block. The pulse applied to the e field at all points along the mesh boundaries for a time τ_c effectively simulates Neumann boundary conditions for the block bounded by the mesh, thus spirals formed inside the block are absorbed at the mesh bounding the block. For $d = 2$, $L = 128$, and $K = 2$, a time $\tau_c = 41.2$ ms is required for defibrillation. When $L = 512$, and $K = 8$, a time $\tau_c = 704$ ms is required. Electrical pulses of amplitude $\cong 60\ \mu A/cm^2$ are applied to the control mesh, which is much less than in conventional electrical defibrillation which uses pulses of amplitude 1 A/cm^2. This control algorithm has been extended to suppress spiral turbulence initiated in the three-dimensional Panfilov and two-dimensional BR and LR models[12]. To apply this control algorithm in the three-dimensional Panfilov model directly, one needs a cubic array of sheets. However, such an array of control sheets cannot be implanted easily in a ventricle. But it was shown in ref. [7] that, even if the control mesh is present only on one of the $L \times L$ faces of the $L \times L \times L_z$ domain, the above scheme will work provided that $L_z \leq 4$. A slight modification of this scheme is effective even for $L_z > 4$: Instead of applying a pulse for a duration τ_c, apply a sequence of n pulses separated by a time τ_{ip}, with each pulse of duration τ_w. Control via a steady pulse does not work for $L_z > 4$ since the propagation of this pulse in the z direction is blocked once the medium in the interior of the simulation domain becomes refractory. However, if we use a sequence of short pulses separated by a time τ_{ip}, then, provided τ_{ip} is long enough for the medium to recover its excitability, the control-pulse waves can propagate in the z direction and lead to successful defibrillation. Hence optimal defibrillation is obtained in the model if τ_{ip} is equal to the absolute refractory period of the model without the Laplacian term. We refer the reader to refs. [7,12] for further details.

4 Conclusion

Although many practical difficulties remain to be overcome, the recent understanding of cardiac arrhythmias developed in the context of spiral turbulence and spatiotemporal chaos in partial-differential equation models offers hope for developing clinically useful defibrillation techniques. Conventional methods of defibrillation have many disadvantages. The application of high voltages across the heart is often painful. It can cause burns in the heart tissue, creating scars, which may act as the nuclei for anatomical reentry and yet another episode of fibrillation. Thus low-amplitude defibrillation techniques are very appealing. The method of controlling VF suggested in refs. [7,12] should therefore be tested experimentally both in *vitro* and *in vivo* for applicability in clinical setting.

5 Acknowledgements

One of the author (TKS) would like to thank CSIR (India) for support. The authors also thank SERC (IISc, Bangalore) for computational facilities, the Department of Science and Technology (India) for support, and Profs A Pande and A Sen for discussions.

Appendix A : The Beeler-Reuter Model

In the Beeler-Reuter (BR) model there are four individual components of ionic current, which are formulated mathematically in terms of Hodgkin-Huxley-type equations. The model incorporates two voltage- and time-dependent inward currents, the excitatory inward sodium current, I_{Na}, and a secondary or slow inward current, I_s, primarily carried by calcium ions. A time-independent outward potassium current, I_{K_1}, exhibiting inward-going rectification (i.e., the current activates only when V_m is negative), and a voltage- and time-dependent outward current, I_{x_1}, primarily carried by potassium ions, are further elements of this model. Without the diffusion term, the transmembrane potential obeys the equation

$$\frac{dV_m}{dt} = \frac{-1}{C_m}\,(I_{K_1} + I_{x_1} + I_{Na} + I_s - I_{external}), \qquad \ldots(A1)$$

where C_m is the membrane capacitance density, taken as $1\,\mu F/cm^2$ in this model, and $I_{external}$ is the external stimulus current.

The currents are defined as

$$I_{K_1} = 0.35\frac{4(\exp[0.04(V_m+85)]-1}{(\exp[0.08(V_m+53)]+\exp[0.04(V_m+53)])} + \frac{0.2(V_m+23)}{(1-\exp[-0.04(V_m+23)])}, \qquad \ldots(A2)$$

$$I_{Na} = (G_{Na}m^3hj + G_{NaC})\,(V_m - E_{Na}), \qquad \ldots(A3)$$

$$I_{x_1} = 0.8x_1\frac{\exp[0.04(V_m+77)]-1}{\exp[0.04(V_m+35)}\mathrm{y}, \qquad \ldots(A4)$$

the sodium conductance $G_{Na} = 4$, $G_{Nac} = 0.003$, and the Nernst potential for sodium ions $E_{Na} = 50$. The slow inward current is

$$I_s = G_s df\,(V_m - E_s), \qquad \ldots(A5)$$

where $G_s = 0.09$, and

$$E_s = -82.3 - 13.0287 \ln[Ca]_i, \quad ...(A6)$$

with $[Ca]_i$ the calcium ion concentration inside the cell.

All currents are in $\mu A/cm^2$, voltage are in mV, conductances (g) are in mmho/cm^2, and x_1, m, h, j, d, and f are dimensionless. The membrane potential V_m is taken as the difference between the potentials inside and outside the cell. The calcium concentration obeys the ordinary differential equation

$$\frac{d[Ca]_i}{dt} = -10^{-7} I_s + 0.07(10^{-7} - [Ca]_i) \quad ...(A7)$$

and the rate constants are [eq. (2)]

$$\alpha_{x_1} = \frac{0.0005\exp[0.083(V_m+50)]}{\exp[0.057(V_m+50)+1}, \quad ...(A8)$$

$$\beta_{x_1} = \frac{0.0013\exp[-0.06(V_m+20)]}{\exp[-0.04(V_m+20)+1}, \quad ...(A9)$$

$$\alpha_m \frac{-(V_m+47)}{\exp[-0.1(V_m+47)]-1}, \quad ...(A10)$$

$$\beta_m = 40 \exp[-0.056(V_m + 72)], \quad ...(A11)$$

$$\alpha_h = 0.126 \exp[-0.25(V_m + 77)], \quad ...(A12)$$

$$\beta_h = \frac{1.7}{\exp[-0.082(V_m+22.5)]+1}, \quad ...(A13)$$

$$\alpha_j = \frac{0.055\exp[-0.25(V_m+78)]}{\exp[-0.2(V_m+78)]+1}, \quad ...(A14)$$

$$\beta_j = \frac{0.3}{\exp[-0.1(V_m+32)]+1}, \quad ...(A15)$$

$$\alpha_d = \frac{1}{\sigma}\frac{0.095\exp[-0.01(V_m-5)]}{\exp[-0.072(V_m-5)]+1}, \quad ...(A16)$$

$$\beta_d = \frac{1}{\sigma}\frac{0.07\exp[-0.017(V_m+44)]}{\exp[0.05(V_m+44)]+1}, \quad ...(A17)$$

$$\alpha_f = \frac{1}{\sigma}\frac{0.012\exp[-0.008(V_m+28)]}{\exp[0.15(V_m+28)]+1}, \quad ...(A18)$$

$$\beta_d = \frac{1}{\sigma}\frac{0.0065\exp[-0.02(V_m+30)]}{\exp[-0.2(V_m+30)]+1}. \quad ...(A19)$$

To account for spatial coupling we need to introduce a diffusion term in the eq. (A1), namely,

$$\frac{\partial V_m}{dt} = \frac{-I_{BR}}{C_m} + D\nabla^2 V_m, \quad ...(A20)$$

where $I_{BR} + I_{k1} + I_{x1} + I_{Na} + I_s - I_{external}$.

Appendix B : The Luo-Rudy Model

The Luo-Rudy (LR) model is similar to the BR model except in the details of the ionic current I_{LR}. The partial differential equation for this model is

$$\frac{\partial V}{\partial t} + \frac{I_{LR}}{C} = D\nabla^2 V. \quad ...(B1)$$

Here I_{LR} is the instantaneous, total ionic-current density. The subscript LR denotes that we use the formulation of the total ionic current described by the Luo-Rudy Phase I (LR1) model[25]. In the LR1 model, $I_{LR} = I_{Na} + I_{si} + I_K + I_{K1} + I_{Kp} + I_b$. Here

$$I_{Na} = G_{Na} m^3 hj\ (V - E_{Na}) \quad ...(B2)$$

is the fast inward Na^+ current density,

$$I_{si} = G_{si} df\ (V - E_{si}) \quad ...(B3)$$

is the slow inward current density,

$$I_K = G_K x x_1\ (V - E_K) \quad ...(B4)$$

is the slow outward *time-dependent* K^+ current density,

$$I_{K_1} = G_{K_1} K_{1\infty}(V - E_{K_1}) \quad ...(B5)$$

is the *time-independent* K^+ current density, and $K_{1\infty}$ is the steady-state value of the gating variable K_1,

$$I_{Kp} = G_{Kp} K_p\ (V - E_{Kp}) \quad ...(B6)$$

is the plateau K^+ current density, and

$$I_b = 0.03921\ (V + 59.87) \quad ...(B7)$$

is the total background current density. All current densities are in units of $\mu A/cm^2$, voltages are in mV and G_ξ and E_ξ are, respectively, the ion-channel conductance and reversal potential for the channel ξ. The ionic currents are determined by the time-dependent ion-channel gating variables h, j, m, d, f, x, x_1, K_p and K_1 generically denoted by ξ, which follow ordinary differential equations of the type

$$\frac{d\xi}{dt} = \frac{\xi_\infty - \xi}{\tau_\xi}, \quad ...(B8)$$

where $\xi_\infty = \alpha_\xi/(\alpha_\xi + \beta_\xi)$ is the steady-state value of ξ and $\tau_\xi = \frac{1}{\alpha_\xi + \beta_\xi}$ is its time constant. The voltage-dependent rate constants, α_ξ and β_ξ, are given by the following empirical equations :

$$\alpha_h = 0, \text{ if } V \geq -40 \text{ mV},$$
$$= 0.135 \exp[-0.147(V+80)], \text{otherwise}; \quad ...(B9)$$

$$\beta_h = \frac{1}{0.13\ (1+\exp[-0.09(V+10.66)])},$$
$$\text{if } V \geq -40 \text{ mV},$$
$$= 3.56 \exp[0.079\ V] + 3.1 \times 10^5\ exp[0.35\ V], \text{otherwise}; \quad ...(B10)$$

$$\alpha_j = 0, \text{ if } V \geq -40 \text{ mV},$$
$$= \left[\frac{(\exp[0.2444V] + 2.732\times10^{-10}\exp[-0.04391\ V])}{-7.865\times10^{-6}\ \{1+\exp[0.311\ (V+79.23)]\}}\right] (V + 37.78), \text{otherwise}; \quad ...(B11)$$

$$\beta_j = \frac{0.3 \exp[-2.535 \times 10^{-7} V]}{1+\exp[-0.1\,(V+32)]}, \text{ if } V \geq -40 \text{ mV},$$

$$= \frac{0.1212 \exp[-0.01052\,V]}{1+\exp[-0.1378\,(V+40.14)]}, \text{ otherwise;} \quad ...(B12)$$

$$\alpha_m = \frac{0.32\,(V+47.13)}{1-\exp[-0.1\,(V+47.13)]}; \quad ...(B13)$$

$$\beta_m = 0.08 \exp[-0.0909\,V]; \quad ...(B14)$$

$$\alpha_d = \frac{0.095 \exp[-0.01\,(V-5)]}{1+\exp[-0.072\,(v-5)]}; \quad ...(B15)$$

$$\beta_d = \frac{0.07 \exp[-0.017\,(V+44)]}{1+\exp[0.05\,(V+44)]}; \quad ...(B16)$$

$$\alpha_f = \frac{0.012 \exp[-0.008\,(V+28)]}{1+\exp[0.15\,(V+28)]}; \quad ...(B17)$$

$$\beta_f = \frac{0.0065 \exp[-0.02\,(V+30)]}{1+\exp[-0.2\,(V+30)]}; \quad ...(B18)$$

$$\alpha_x = \frac{0.0005 \exp[0.083\,(V+50)]}{1+\exp[0.057\,(V+50)]}; \quad ...(B19)$$

$$\beta_x = \frac{0.0013 \exp[-0.06\,(V+20)]}{1+\exp[-0.04\,(V+20)]}; \quad ...(B20)$$

$$\alpha_{K1} = \frac{1.02}{1+\exp[0.2385\,(V-E_{K1}-59.215)]}; \quad ...(B21)$$

$$\beta_{K1} = \frac{[0.49124 \exp[0.08032\,(V-E_{K1}+5.476)]}{1+\exp[-0.5143\,(V-E_{K1}+4.753)]} + \exp[0.06175\,(V-E_{K1}-594.31)]. \quad ...(B22)$$

the gating variables x_i and K_p are given by

$$x_i = \frac{2.837 \exp 0.04(V+77)-1}{(V+77)\exp 0.04\,(V+35)}, \text{ if } V > -100\text{mV},$$

$$= 1, \text{ otherwise;} \quad ...(B23)$$

$$K_p = \frac{1}{1+\exp[0.1672\,(7.488-V)]}. \quad ...(B24)$$

The values of the channel conductances G_{Na}, G_{si}, G_K, G_{K1}, and G_{Kp} are 23, 0.07, 0.705, 0.6047 and 0.0183 mS/cm^2, respectively[41]. The reversal potentials are E_{Na} = 54.4 mV, E_K = – 77 mV, $E_{K1} = E_{Kp}$ = – 87.26 mV, E_b = –59.87 mV, and E_{si} = 7.7 – 13.0287 ln Ca, where Ca is the calcium ionic concentration satisfying

$$\frac{dCa}{dt} = -10^{-4} I_{xi} + 0.07(10^{-4} - Ca). \quad ...(B25)$$

The times t and τ_ξ are in ms; the rate constants α_ξ and β_ξ are in ms^{-1}.

References

1 American Heart Association *Heart and Stroke, Statistical Update* (AHA Dallas 2001)

2 BBC Health News (http://news.bbc.co.uk/2/hi/health/248229/.stm) Nov 18, 2002

3 J Jalife, R A Gray, G E Morley and J M Davidenko *Chaos* **8** (1998) 79; R A Gray, A M Pertsov and J Jalife *Nature (London)* **392** (1998) 75, F X Witkowski, L J Leon, P A Penkoske, W R Giles, M L Spano, W L Ditto and A T Winfree *Nature (London)* **392** (1998) 78

4 G P Mines *J Physiol (London)* **46** (1913) 349; W E Garrey *Amer J Physiol* **33** (1914) 397

5 W E Garrey *Physiol Rev* **4** (1924) 215

6 M A Allessie, F I M Bonke and F J C Schopman *Circ Res* **33** (1973) 54

7 S Sinha, A Pande and R Pandit *Phys Rev Lett* **86** (2001) 3678

8 M Hiderband, M Bär and M Eiswirth *Phys Rev Lett* **75** (1995) 1503; M Bär and M Eiswirth *Phys Rev E* **48** (1993) R1635

9 B N Vasiev, P Hogeweg and A V Panfilov *Phys Rev Lett* **75** (1994) 3173

10 J Murray *Mathematical Biology* Springer-Verlag Verlin 1998

11 A T Winfree *When Time Breaks Down* Princeton University Press Princeton (1987)

12 R Pandit, A Pande, S Sinha and A Sen *Physica A* **306** (2002) 211

13 W A H Rushton *Proc R Soc Lond* (Biol) **124** (1937) 210

14 A Kolmogorov, I Petrovsky and N Piscounoff *Bull Univ Moscow Math Serie Int* **A.1** (1937) 1

15 K S Cole *Membranes, Ions and Impulses* University of California Press (1972)

16 A L Hodgkin and A F Huxley *J Physiol (London)* **117** (1952) 500

17 D Noble *Nature* **188** (1960) 495; D Noble *J Physiol* **160** (1962) 319

18 G W Beeler and H J Reuter *J Physiol* **268** (1977) 177

19 R FitzHugh *Biophys J* **1** (1961) 445; J Nagumo, S Arimoto and S Yoshizawa *Proc IRE* **50** (1962) 2061

20 G Bug, A Shrier and L Glass *Phys Rev Lett* **88** (2002) 058101

21 G K Moe, J A Abildskov and J Han *Amer Heart J* **67** (1964) 200

22 M Malik and A J Camm *Cardiovasc Res* **20** 436 (1986)

23 R H Mitchell, A Bailey and J Anderson *IEEE Trans Biomed Eng* **39** (1992) 253

24 R H Clayton *Physiol Meas* **22** (2001) R15

25 C H Luo and Y Rudy *Circ Res* **68** (1991) 1501

26 J Jalife *Basic Cardiac Electrophysiology for the Clinician* Futura Publishing Co (1999)

27 C H Luo and Y Rudy *Circ Res* **74** (1994) 1071; L Priebe and D J Beuckelmann *Circ Res* **82** (1998) 1206

28 M Courtemanche *Chaos* **8** (1998) 57

29 A V Panfilov and P Hogeweg *Phys Lett A* **176** (1993) 295

30 A V Panfilov *Chaos* **8** (1998) 57

31 T K Shajahan, S Sinha and R Pandit *Int J Mod Phys B* **17** (2003) 5645

32 A Pande, S Sinha and R Pandit *J Indian Inst Sci* **79** (1999) 31
33 R Pool *Science* **247** (1990) 1294
34 A Garfinkel, M L Spano, W L Ditto and J N Weiss *Science* **257** (1992) 1230
35 V N Biktashev and A V Holden *Chaos* **8** (1998) 48
36 G V Osipov and J J Collins *Phys Rev E* **60** (1999) 54
37 W J Rappel, F Fenton and A Karma *Phys Rev Lett* **83** (1999) 456
38 Y H Kim, A Garfinkel, T Ikeda, T J Wu, C A Athill, J N Weiss, H S Karagueuzian and P S Chen *J Clin Invest* **100** (1997) 2486
39 A G Mayer *Papers from the Marine Biological Laboratory at Tortugas* Carnegie Institution of Washington Publication No. 102 (1908)
40 R A Gray and J Jalife *Circulation* **94** (1996) 1
41 Z Qu, J N Weiss and A Garfinkel *Am J Physiology: Heart Circ Physiol* **276** (1999) H269